Lunar megaregolith mixing by impacts: Evaluation of the non-mare component of mare soils

Tiantian Liu[1,3], Greg Michael[2], Wilhelm Zuschneid[2], Kai Wünnemann[2,3], Jürgen Oberst[1,4]

[1] Institute of Geodesy and Geoinformation Science, Technische Universität Berlin, 10623 Berlin, Germany (tiantian.liu@tu-berlin.de)

[2] Freie Universität Berlin, Malteserstr., 74-100, Haus D, 12249 Berlin, Germany

[3] Museum für Naturkunde, Leibniz Institute for Evolution and Biodiversity Science, 10115 Berlin, Germany

[4] Institute of Planetary Research, German Aerospace Center (DLR), 12489 Berlin, Germany

Key words:

Moon, surface; Regoliths; Impact processes; Cratering

Abstract

The source of the non-mare component in the lunar mare soil samples is still an open question. A spatially-resolved numerical model tracing the diffusion of non-mare material was developed by means of the Monte Carlo method to study this issue in more detail. The vertically- and laterally-transported non-mare components are recorded separately to assess their concentration on the surface. We find a general higher efficiency of lateral transport than of vertical transport, but the opposite may occur within small zones of interest. The overall (background) distribution of non-mare component is estimated by averaging out regional variations of material composition caused by local impact mixing. We find that almost all the mare surface is mixed with non-mare material. If most of the mare regions have filled basaltic material about 500 m in thickness since the formation of basins, the average non-mare fraction in the top 5 m is about 0.1. The abundance of the non-mare component decreases with increasing distance from the mare-highland boundary, but the slope of the distance-dependence is shallower within ~100 km of the boundary than further away.

By comparing the background composition derived from our model with the geochemical analysis and geological interpretation of the lunar mare soil samples, we infer the most plausible geologic processes that have significantly altered the material composition at the sampling sites: for the Apollo 15 and 17 mare soil samples, the large fraction of non-mare material is likely to have resulted from the downslope slumping or lateral transport of the nearby massifs. The Apollo 12 sampling site that is located interior domains of Oceanus Procellarum has a component of Copernicus ejecta. A mixing of both Copernicus ejecta and excavated local underlying material by high-velocity ejecta has altered the composition at the surface. The non-mare material contained in the Apollo 11 and Luna 24 mare soil samples could have been built up gradually by both long-time lateral and vertical mixing. The mare deposit at the Luna 16 landing site is likely to be

relatively thin resulting in the abundant vertically transported non-mare component. Since the history of the lunar volcanic eruptions - deposit thicknesses, flux curves and onset of activity - have not been well constrained, we make simple estimates with the first-order accuracy. In addition, it was found that the vertically transported non-mare abundance in the top surface is influenced by both the cessation time of the major mare fillings and the total amount of mare deposit; the laterally-transported non-mare abundance in the top surface is mainly dependent on the cessation time of the major mare fillings. The peak time of eruption would not change the abundance of both the laterally and vertically transported non-mare component.

1. Introduction

1.1. Non-mare component in the lunar mare soil samples

The returned lunar mare soil samples consist not only of local mare basalts but also of highland anorthosites (Wood, 1970). We use the term *non-mare* to refer to the components that are clearly not of volcanic mare origin but for which the relationship to the highlands is not clear or firmly established (e.g., Warren & Wasson 1977). The amount of non-mare material in Apollo 11, 12, and Luna 16 mare soil samples is about 20% on average; some of the Apollo 12 soil samples have more than 70% non-mare material (Rhodes, 1977). In addition, data from the orbital X-ray experiments (the measurement depth for the X-ray data is about 20 μm; Lucey et al. 2006) indicated that, for most mare surfaces, the chemical compositions, such as Al/Si concentration ratios, are more comparable with that obtained from the analyzed mare soils than with that of the local basalts. Thus it was suggested that the mixture of non-mare component in mare soils was not only restricted to the sampling sites that are near the mare margins, but may be a mare-wide phenomenon (Trombka *et al.*, 1974; Rhodes, 1977; Prettyman *et al.*, 2006).

The source of the non-mare component contained in the mare samples has been debated since the Apollo epoch (Rhodes, 1977; Laul and Papike, 1980; Simon, Papike and Laul, 1982; Farrand, 1988; Fischer and Pieters, 1995; Li and Mustard, 2000; Huang *et al.*, 2017). Two hypotheses have been proposed: It could result mainly from the mixing of material transported laterally by impacts from the distant highland regions (De Hon, 1974; Head, 1982; Budney and Lucey, 1998; Evans *et al.*, 2016). It could also primarily be result from the mixing with local material that originally occurred beneath the mare deposit and was excavated by impact events (Arvidson *et al.*, 1975; Rhodes, 1977; Hörz, 1978; Laul and Papike, 1980; Fischer and Pieters, 1995). Studies of both remote sensing data and collected samples have been used to evaluate the efficiency of lateral and vertical transport. The material mixing process across mare-highland contacts driven by a great number of impact events results in a mixing zone inside mare regions where the surface material has been mixed with a significant amount of non-mare component displaying relative high albedo in optical images. The observed ~4-5 km wide mixing zone across the mare-highland boundary is relatively narrow, indicating inefficient lateral mixing by impact events, while the abundance of highland material in the soil samples far from this boundary suggests more efficient lateral transport.

Huang et al. (2017) implemented a regolith material transport model into the Cratered Terrain Evolution Model (CTEM) to investigate the mixing of material across the mare-highland boundary.

The effects of local and distal ejecta were systematically studied and their relatively importance was quantified. It was found that both local and distal material transports were important to the material diffusion across the mare-highland boundary. In addition, the superposition of crater rays was proposed to be a likely cause for the elevated non-mare abundance in some mare soil samples. For example, the Apollo 12 soil samples that had a significantly higher concentration of non-mare component were suggested to be influenced by the emplacement of the Copernicus Crater ray material.

While the research of Huang et al. (2017) has improved our understanding of non-mare diffusion over the lunar surface, there remain several issues to resolve. First, Huang took the mare deposit as an intact layer on top of a highland layer. But the mare flooding occurred intermittently. Earlier transported non-mare material could become buried decreasing its abundance on the surface. Furthermore, the non-mare components beneath the mare deposit were not traced. Therefore, the relative magnitude of lateral versus vertical transport could not be evaluated.

In this study, we aim to develop a numerical model to trace the diffusion of non-mare material with the cumulative effect of impact mixing and intermittent filling of mare material. Questions that need resolving are: (a) Was the non-mare component transported over large distances on to the mare surfaces following the emplacement of mare material? Or (b) did a significant fraction of it originate beneath the mare surface? (c) How do spatial and temporal variations in mare deposition affect the expected surface abundances of non-mare materials today?

1.2. Mare volcanic flooding

Besides the impact mixing process, the volcanic eruptions are a key process to model. Previous work, nevertheless, has shown the difficulty to establish a well-constrained eruption flux (e.g., Head & Wilson 1992; Wilson & Head 2017; Hiesinger, Head, *et al.,* 2011).

In order to constrain the flux of mare volcanism, the thicknesses of individual flows are required, which are found on the basis of their morphometric characteristics neglecting the problem that most flows are covered by others. Such measurements, nevertheless, are complicated due to the limited availability of suitable data necessary for the recognition of flow fronts (i.e. high-resolution topography and low-sun images), and the obliteration of flow fronts caused by impact cratering.

The onset and duration of mare volcanism are not well understood (summarized by Niquist et al. 2001). The returned samples revealed that mare volcanism was active between ~3.9 and 3.1 Ga (Head, 1976; Nyquist and Shih, 1992). The ages of some basaltic clasts in older breccias point to an onset of mare volcanism prior to 3.9 Ga (Ryder and Spudis, 1980), perhaps as early as 4.2–4.3 Ga (Taylor *et al.*, 1983; Dasch *et al.*, 1987; Nyquist, Bogard and Chi-Yu, 2001). Dark halo craters found in remote sensing data may support the presence of the older volcanism. These craters are interpreted to be impacts into basaltic deposits that are now buried underneath a veneer of basin ejecta. These underlying basalts might be among the oldest mare material on the Moon (Schultz and Spudis, 1979; Hawke and Bell, 1982). In addition, crater counts on mare surfaces suggest that some mare volcanism erupted as late as ~1–2 Ga ago (Hiesinger, Head, *et al.*, 2011), which is much younger than that was determined in the collected samples (~3 Ga).

The total thickness/volume of the volcanic deposits is an important quantity in defining the extent of mare volcanism. A variety of techniques have been applied to estimate the total volume, but no consistent results have been obtained. Crater-geometry techniques using pristine crater morphometric relationships and the diameter of partially to almost entirely flooded craters yield values of mare thickness up to 2 km, ranging 200–400 m on average (De Hon, 1974, 1979; De Hon and Waskom, 1976; Hörz *et al.*, 1991). Hörz (1978) further refined the crater-geometry technique by considering the average degradational state of impact craters, and argued that the mare thicknesses estimated by De Hon and coworkers should be decreased by a factor of ~2. Other constraints are derived from "mascons" (i.e. the positive gravity anomalies observed over many of the basins filled with mare material). When the excess mass required to produce the observed gravity anomaly is assumed to be entirely mare filling, estimates for mare thickness of 1–2 km are obtained (Phillips *et al.*, 1972; Phillips and Lambeck, 1980; Solomon and Head, 1980). However, these are minimum estimates, because it is not known whether there is additional mare fill below the equilibrium gravitational surface used in the modeling. In addition, there would be at most ten times larger estimates of the total volume if one assumes a specific geometry for the original impact basin cavities, modeled after the Orientale basin, and assumes similar cavity geometries for the all basins (Head, 1977).

Since higher-quality image data are now available, more studies have been done aiming to estimate the basaltic thickness. For example, by using recent high-resolution topographic data, Du *et al* (2019) revisited the previous studies of De Hon and Hörz. They identified 661 buried craters over the lunar surface and concluded that the basaltic thicknesses vary from 33-455 m with a medium value of 105 m. Using the high-resolution gravity and topography data, Gong *et al.* (2016) estimated the total thickness of basalts on the nearside hemisphere, which yield an average thickness of 740 m. In addition, a recent study from Needham & Kring (2017) summarized the thickness estimate of Williams & Zuber (1998) and some other recent estimates to calculate the volume of mare deposit. They derived a thinner average mare thickness of ~250 m.

Both the duration of emplacement and the thickness of mare deposits are not precisely known making it difficult to estimate the eruption flux. Our goal is thus to estimate the diffusion pattern of the non-mare material from different sources. In section 2, the main aspects of the previously developed model are outlined and the integration of the lunar volcanic history into it is described.

In section 3 and 4, two cases including the rapid and continuous mare fillings are present. First, and more simply (section 3), we take the volcanic material to be emplaced instantaneously as single layers. Secondly (section 4), we investigate a probably more realistic scenario, where the mare material slowly and continuously fills the basins. To investigate the diffusion features of the lateral and vertical mixing, the abundances of the laterally and vertically transported components are traced separately, and the relative rates of lateral versus vertical transport are evaluated. In section 5, the overall distribution of non-mare material is presented. Based on the model-predicted non-mare abundance, the origin of the non-mare component in the mare samples is discussed in section 6.

2. Model

In our previous work (Liu *et al.*, 2020), a spatially-resolved numerical model was developed to investigate the diffusion of impact melts through impact mixing. Using the Monte Carlo method, a sequence of impact events was generated, where the occurrence time and the size of impact craters were calculated on the basis of the chronology and production functions of Neukum (1983). In the model, impact events of different sizes occurred in sequence. The occurrence of each impact event would exhume some local (target) material. The excavation depth, d_{exc}, was approximated to one third of the transient crater depth. The volume of the excavated materials was estimated to be one-third of a disc with d_{exc} in thickness and the transient crater size in diameter. The excavated material would be emplaced outside the crater cavity as ejecta layers, the thickness of which decreases with distance from crater center. In addition, the high-velocity ejecta would mix with local material while emplacing. The degree of mixing was quantified using a mixing ratio of local material to ejecta, $\mu = 0.0183r^{0.87}$ (Oberbeck *et al.* 1975). When μ is larger than 5.0, the value of μ was modified by roughly half: $\mu' = \mu/2 + 2.5$ (Petro & Pieters 2006).

The evolving distribution of material composition on the surface and with depth caused by each impact event was recorded by the uniformly distributed one million points on a sphere with the Moon's radius (1737.4 km). Each point was related to a certain area of ~5×5 km^2. In addition, the increasing number of deposition layers as the simulation progresses made it necessary to periodically simplify the layer sequence to one: 0.2×1.9^a m, where a = 0, 1, …, 20. Materials within set layers would be mixed together resulting in a more average composition. The thinner layers close to the surface were chosen to preserve a fine resolution of material composition in the near surface. A more detailed explanation of the model is given in Liu et al. (2020).

In this study, we extend the capabilities of the model and take into account the volcanic basin infilling forming the lunar mare regions. The minimum crater diameter considered is 5 km. In the following section, the models used to simulate the ejecta distribution and the mare fillings are presented in detail. In all model runs of sections 3 and 4, the simulated cratering is identical in timing, position, and crater sizes, so all changes can be attributed to the varying parameters of the lava emplacement process.

2.1. Ejecta distribution

During the formation of an impact crater, the majority of the excavated material is deposited near the crater rim forming a continuous blanket (i.e. the proximal ejecta which is generally distributed within 2-3 radii from the crater center). Further away from the crater, the continuous ejecta is replaced by the patchily distributed distal ejecta, usually in the form of bright rays and grouped secondary craters. Although the volume of distal ejecta is not large (~25% deposits further than five radii away from the transient crater rim; Liu *et al.*, 2019, 2020), previous studies have shown its significance to the material composition of mare regions. For example, the study of Huang et al. (2017) focused on the diffusion of non-mare material across the mare-highland contact. It showed that if only the proximal ejecta contributed to the soil composition, the mare surface would be clearly different from what is actually seen on the Moon, and the mare-highland mixing zone would be rather narrower than observed.

For proximal ejecta, the thickness distribution with distance from crater center (r) conforms to a power law, typically: $\delta(r) = Ar^{-3}$ (A is constant but varies for differently-sized craters, Melosh 1989). However, so far, no systematic research has been performed to obtain a scaling law for the thickness distribution of distal ejecta. In addition, distal ejecta may occur much further out than where we see bright rays and secondary craters. This fraction of the distal ejecta emplaced with high velocity and fine grain size is difficult to distinguish from the background surface.

Places superposed by the patchy distal ejecta locally have thicker transported material than their surrounding background. This clustered material would be redistributed by the subsequent impact events. As time passes, the clustered material diffuses over the larger area decreasing the thickness. That is, the patchy distal ejecta would fade into the background with continuous impact mixing, and the thickness distribution of the patchy ejecta material becomes more uniform. The average effect on distal ejecta looks similar to a uniform distribution. To estimate the distribution of distal ejecta, we therefore assume that the distal ejecta is also continuously distributed, and the thickness is calculated based on the extrapolated power law mentioned above. Although the distal ejecta of recently-formed larger impact craters, such as Copernicus crater, could still remain patchy, their regional influence could be easily recognized from their background. If it occurs over the target regions, such as sampling sites, the composition of regional surface could be significantly different from its background.

The power-law distribution of ejecta thickness leads to a thinner deposit at locations further from the impact center. The farthest ejecta that the model would trace should thus have the minimum deposit thickness ($h_{\min}$), based on which the ejecta coverage range of each impact event can be calculated. All the excavated material would be distributed within the coverage range to maintain the total volume. The value of $h_{\min}$ is taken to be 0.01 m in this study. Our simulations showed that a smaller value for the minimum thickness, which would relate to a larger traced range of ejecta, would lead to a similar composition of surface material since the volume of ejecta at greater ranges becomes too small to significantly augment the non-mare component. For example, when the value of $h_{\min}$ is ten times smaller (i.e., 0.001 m), the estimated composition of surface material is comparable with that using $h_{\min}$ of 0.01 m, and the difference of non-mare fraction in the near surface is generally smaller than ~0.001. On the other hand, a larger value of $h_{\min}$ would relate to a smaller range of ejecta deposit. The simulation results then display significantly less mixing of the non-mare component over the mare regions. For example, when the value of $h_{\min}$ is ten times larger (i.e., 0.1 m), more than half of the mare surface, especially the central part of mare regions, has no mixing of non-mare material. This is clearly not in agreement with the observed composition of the lunar surface, so that we exclude this value. The simulation results with the varying values of $h_{\min}$ are presented in the supplementary file.

Craters smaller than 5 km are not involved in the model. The smaller impact events have high frequency. They have well mixed the material in the top surface producing a fragmental regolith layer. However, since they hardly excavate fresh material from the beneath maria, they would not significantly change the abundance of the material components in the top surface. Given that the typical thickness of regolith layer over the maria is about 5 m (McKay et al., 1991; Fa and Jin, 2010; Fa et al., 2014), in the following discussions, we present the average abundance of non-mare component in the top 5 m. These results can be regarded as the average composition of the regolith where the material has been frequently mixed by smaller impact events and hence the material is homogeneously distributed.

2.2. Mare volcanic filling

As indicated by the diverse basalt ages over the mare regions (e.g., 30 units over Mare Imbrium; Hiesinger, Head, *et al.,* 2011), the lunar basins were filled with multiple flow units. The intermittent mare flooding would decrease the distribution of early-transported non-mare component on the surface. Therefore, as well as the impact mixing process, the sequential mare volcanic filling is also described by the model. The way to simulate both processes is illustrated in Figure 1a. Before the flooding by volcanic material, both the highland and mare region surfaces are non-mare material. To better trace the vertical and lateral mixing of the non-mare component, the non-mare component originating from the highland regions is tracked as "laterally" transported non-mare material, and that from beneath the mare infill as "vertically" transported non-mare material. The labels "laterally" and "vertically" are used to specify the spatial origin, but not necessarily a different mineralogical composition.

At the time of a_1 (Figure 1 a1), an eruption occurred, burying the surface of the mare region with volcanic material m_1. Subsequent impact mixing redistributes mare material regionally, and excavated some non-mare materials from beneath the mare layer (i.e. vertically transported non-mare component). Some highland material is transported from the highlands to the mare region (indicated by the arrow in Figure 1 a2). At the time of a_3 (Figure 1 a3), another volcanic eruption occurs, the generated mare material deposits m_2 on the top of volcanic deposit m_1. The impact mixing keeps laterally transporting the non-mare material to the mare regions. Some of the early-formed volcanic deposit m_1 are re-excavated to the surface (the open arrow in Figure 1 a4); some of the early-transported highland could be delivered to the surface (the thick closed arrow in Figure 1 a4); some mare material might be transported to the highlands (the thin closed arrow in Figure 1 a4). On the lunar surface, the long-term impact mixing excavates various amounts of both mare and non-mare material to the surface, resulting in the mixing of mare/non-mare components to different degrees in the present day.

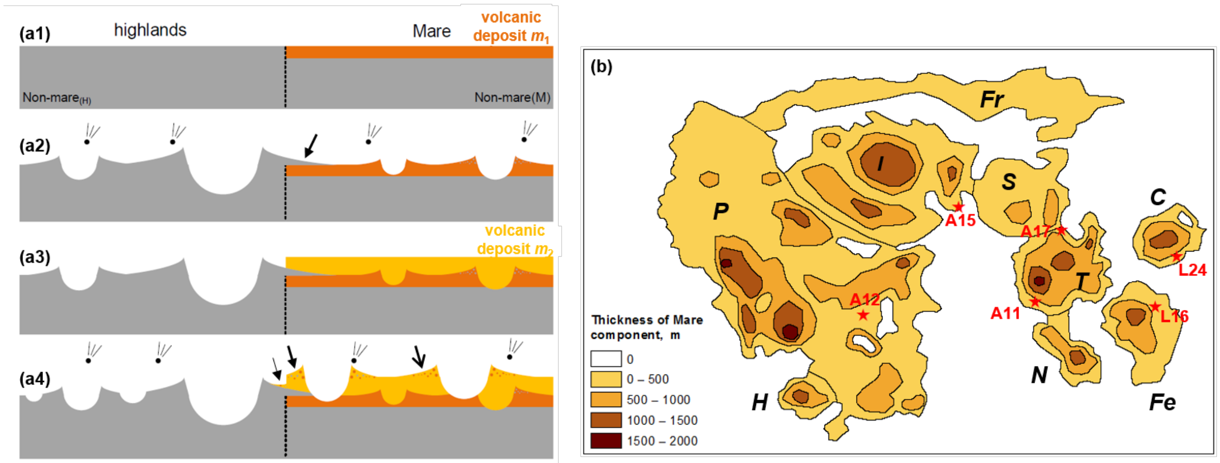

Figure 1 (a1-a4) A schematic of the filling of volcanic material. (b) The thickness distribution of mare material (after De Hon 1974; De Hon 1979; De Hon & Waskom 1976; Hörz et al. 1991) over the Oceanus Procellarum (P), and the Mare Frigoris (Fr), Fecunditatis (Fe), Humorum (H), Imbrium (I), Serenitatis (S), Tranquillitatis (T), Nectaris (N) and Crisium (C). The red stars indicate the locations of Apollo ("A") and Luna ("L") sampling sites.

In this study, the volcanic filling of the larger mare regions on the lunar near side are simulated, including Oceanus Procellarum (P), and the Mare Frigoris (Fr), Fecunditatis (Fe), Humorum (H), Imbrium (I), Serenitatis (S), Tranquillitatis (T), Nectaris (N) and Crisium (C). Other regions are taken to consist of non-mare highland material. The pre-existing topography that is covered over by successive mare layers is not considered beyond what is shown in Figure 1b.

The eruption flux has not been well constrained. We approximate *the peak time of eruption*, *the thickness of mare deposits*, and the *cessation time of the major eruptions* for modeling.

Peak time of eruption: The qualitative eruption features of volcanic history of the Moon were pictured previously (Head and Wilson, 1992, 2017; Wilson and Head, 2017). Head & Wilson (1992) compared the flux of volcanic filling derived from different approaches (i.e. the volume of mare material emplaced on the surface as a function of time), all of which pictured a similar trend of eruption flux from high to low but with different peak times. Based on the returned samples, a peak prior to ~3.5 Ga was obtained. The recent study from Needham and Kring (2017) that combined the estimated of mare thickness using different methods also indicted the volume peak at ~3.5 Ga. Using the age of the surface exposure of mare units, the flux curve was shifted toward younger ages with the peak at ~3.2 Ga because the older mare material was covered by the uppermost young deposits. Investigations of the stratigraphy of mare material showed the volumetric significance of early mare deposits yielding a flux curve with a peak at older ages of ~ 3.8 Ga. The peak of 3.8 Ga is taken for simulations, and the influence of the younger peak would be discussed in section 4.3.

Thickness of mare deposits: There is no direct measurement of the thickness of lava deposits over the mare regions. The thickness distribution of volcanic deposits was systematically studied using crater-geometry techniques pioneered by De Hon. This approach relies on impact craters flooded by mare material. By using the ideal crater shapes, one can calculate the height of the fresh crater rim. The thickness of mare deposits is then calculated by subtracting the present height from the estimated initial rim height. This approach has been used all observable flooded craters, and isopach maps of the thickness of volcanic filling (Figure 1b) were constructed (De Hon 1974; De Hon 1979; De Hon & Waskom 1976; Hörz et al. 1991). We use this result as an estimate of the total volcanic deposit over the mare regions (H_{DeHon}). Note that, in Figure 1b, the contour of a certain color represents a range of mare thickness. The upper limit (instead of the median value) of each contour is taken for simulations. In this way, the major mare areas are filled with mare material of 500 m in thickness, which is about the median value of the previous estimates (~100 m – ~1 km). The effect of the varying mare thickness on the non-mare distribution is discussed in section 4.3. For each mare region, the areas showing the thickest mare deposit are flooded first. As time goes on, mare material accumulates according to the eruption flux. The surrounding areas of thinner mare deposit are subsequently flooded. After the deposit of the youngest volcanic eruption, the thickness of volcanic deposit corresponds to H_{DeHon}. A time step of 0.01 Ga is used to simulate such continuous eruption. At each step, the mare filling occurred within a certain contour region is taken to be uniformly emplaced.

For mare deposits with a thickness of 500 m, a 5 km diameter crater would begin to tap the underlying non-mare material, the evidence of which could be found through remote sensing data. Such craters were proposed to possess a ring of low FeO ejecta, where the FeO abundance could be calculated using UV-VIS data from the Clementine mission. For example, Thomson et al. (2009) examined 23 craters on Mare Imbrium >10 km in diameter. Six craters were suggested to penetrate the mare deposit indicated by their surrounding halos of low FeO ejecta. However, due to the small volume of the excavated mare component, the ejecta of a crater that just begins to tap the sub-mare material hardly displays obvious low FeO evidence on the surface.

Cessation time of the major eruptions: The mare regions are the result of volcanic infilling after the formation of the giant basins. The absolute age dating of specific rock samples shows that significant periods of time elapsed between basin formation and extrusion of mare material into the basin, but both the basin ages and the onsets of volcanic infilling are only roughly constrained (Wilhelms, 1987; Head and Wilson, 1992; Hiesinger *et al.*, 2011; Whitten and Head, 2015a, 2015b). At one extreme, volcanic eruptions may be assumed to initiate soon after the formation of the respective basin. On the basis of superposed crater density, Wilhelms (1987) documented the relative ages of the lunar basins. Oceanus Procellarum, Frigoris, Fecunditatis, and Tranquilitatis basins were distinguished to be pre-Nectarian, and their formation time was suggested to be around 4.1 Ga. Humorum and Nectaris basins were classified into the Nectarian Period, with formation times around 3.9 Ga. The age of Serenitatis, Crisium and Imbrium could be determined from the returned lunar samples. Although their radioisotopic ages are still debated, the generally accepted formation times of both Crisium and Serenitatis basin are around 3.9 Ga, with the Imbrium basin about 0.05 Ga younger (Stöffler, 2006).

Each volcanic eruption in the model is taken to cover the entire surface within the contour line. This simplified approach can be considered consistent with the early mare filling events, but not with the last flows due to their smaller volume. Head & Wilson (1992) estimated the volume of mare material during different periods, and showed that the volume of Upper Imbrian deposits was about thirty times greater than those later than of the Eratosthenian Period. In addition, the total coverage area of these younger deposits was six times smaller than that of the earlier deposits. With the aim to investigate the general features of non-mare diffusion, the irregularly distributed young mare deposits are not taken into account in this model. However, the cessation time of the mare filling that could cover the entire mare surface (i.e. the cessation time of major mare flooding) is difficult to estimate. The age of the youngest flows help to constrain the infill age. To determine the rough cessation time of the main filling (t_{end}) among different mare regions, we assess the fraction of area of mare deposits younger than a certain age relative to the whole mare region. We take the value of the fraction to be ½, that is, the age t_{end} marks the age when only half of the exposed area would be covered by younger flows, where the age of mare units was estimated by Hiesinger et al. (2011). For Oceanus Procellarum, Mare Frigoris, Humorum, Nectaris, Fecunditatis, Tranquillitatis, Serenitatis, Crisium, and Imbrium, t_{end} is calculated to be 3.4, 3.5, 3.5, 3.6, 3.6, 3.6, 3.5, 3.3, and 3.3 Ga, respectively. The influence of the varying t_{end} value is discussed in section 4.3.

3. Rapid basin filling

In the first case, the volcanic material is taken to be emplaced instantaneously as a single layer at t_{end} over the different mare regions. The thickness of mare material over all the mare regions is taken to be 500 m, the mare thickness in most mare regions (Figure 1b).

3.1. Mixing of the laterally transported non-mare component

The excavated non-mare component is entrained in the ejecta of impact craters that occur on the highlands, a part of it travels across the mare-highland boundary, and then falls on the mare regions (i.e. laterally transported non-mare component). As time goes on, the laterally transported non-mare component on the mare surface builds up. But the early-transported non-mare material could become buried, being covered by a rapid filling of volcanic material. The size and frequency of later-formed impact events would then determine the abundance of the laterally transported non-mare component of the mare surface. Only impacts occurring near the mare-highland boundary could bring a significant amount of laterally transported non-mare material to the mare regions; the ejecta of those occurring far away hardly reaches the mare regions except from some really large craters. Especially at the central areas of the mare regions, little mixing with laterally transported non-mare material occurs.

Figure 2a represents the spatial distribution of the laterally transported non-mare component in the near surface (the top 5 m). It shows that in almost all the mare regions some laterally transported non-mare component is present. Near the margin of the mare regions, laterally transported non-mare material is more abundant than in the inner part that can only be reached by the ejecta of larger impact events. In addition, because of the longer exposure time after the volcanic flooding, the mare regions with the older t_{end}, such as Mare Tranquillitatis and Nectaris, accumulate more laterally transported non-mare material. But the regional context of the mare region also influences the amount of the accumulated laterally transported non-mare component. A mare region surrounded by highland regions would have a higher accumulation rate. For example, although the volcanic cessation time of Mare Crisium is 0.3 Ga later than that of Mare Tranquillitatis and

Fecunditatis, the surface of those regions displays a comparable abundance of laterally transported non-mare component.

3.2. Mixing of the vertically transported non-mare component

Impact events occurring within the mare regions can penetrate through the mare deposit and excavate underlying non-mare material. These large-scale impact events can exhume a great amount of non-mare material to the near surface (i.e. vertically transported non-mare component), forming non-mare-enriched zones. The smaller impact events with shallower excavation depth do not contribute a significant amount of non-mare material to the near surface, but locally garden the surface material diluting the regional concentration of the vertically transported non-mare component.

Figure 2b presents the spatial distribution of the vertically transported non-mare component in the near surface (the top 5 m). We see that vertically transported non-mare is also widely mixed in the near surface but is less abundant, as indicated by the bluish color in Figure 2b. The distribution is relatively heterogeneous marked by some striking non-mare-enriched zones shown in red. These zones are well-preserved indicating their slow fading rate as a result of the lower impact cratering rate during the recent period (Neukum 1983).

4. Continuous basin filling

In a possibly more realistic simulation, the mare material continuously fills the basins until t_{end}. The value of t_{end} is the same as previously, but the total thickness of the basaltic deposit is equal to H_{DeHon} (Figure 1b). The peak time of mare fillings is 3.8 Ga. Note that the following discussions concerning the abundance of non-mare component is on the basis of those given conditions.

4.1. Diffusion features of non-mare material

When the volcanic material is continuously filling the basins, the volume and therefore thickness of each eruption step is much less. Although the surface laterally transported non-mare material would be covered over repeatedly, the smaller thickness of coverage increases the probability that impact events re-excavate the covered laterally transported non-mare material. Some of the laterally transported non-mare component deposited there earlier can become entrained in the ejecta of subsequent impact craters. This way, it could be repeatedly excavated and migrate upwards and finally to the surface layer.

Given the crater diameters of km-scale in simulations, impact events occur on mare regions can easily penetrate through the mare deposit of hundreds of meters in thickness leading to a comparable picture of the concentration of vertically transported non-mare component with that shown in Figure 2b. But on the regions with thicker mare deposit, the abundance of the mare component on the surface should be significantly increased, so that the relative fraction of the vertically transported component becomes less.

4.2. Magnitude of lateral versus vertical mixing

Figure 2c displays the laterally transported non-mare component in the near surface (the top 5 m). It appears essentially the same as in the case of a rapid filling, indicating that the step-wise transport of the early-deposited non-mare component to the near surface is too inefficient to result in a significant difference in composition. The total volume of laterally transported non-mare component over the mare surface is only ~2% larger relative to that with rapid flooding (Figure 2a and the upper sub-plot of Figure 2e), that is, ~2% more the buried component is re-excavated to the mare surface. As we can see that, the histogram distribution of the difference caused by the continual filling (the lower sub-plot of Figure 2e) is smaller than 1.

Figure 2d shows that there are fewer zones enriched in non-mare material caused by vertical transport over the Oceanus Procellarum and Mare Imbrium regions. This deficiency of vertically transported non-mare material is caused by the thicker mare deposit, as indicated in Figure 1b. Fewer impact events are able to penetrate the mare material, and thus in those cases, the fraction of the vertically transported non-mare component is lower. The total volume of vertically transported non-mare component over the mare surface (the top 5 m) is ~ 20% smaller relative to that with rapid flooding mainly (Figure 2b and the upper sub-plot of Figure 2f) due to the missing of non-mare zones caused by the vertical transport at the south and southeast of Oceanus Procellarum (Figure 2d). The histogram distribution of the difference caused by the continual filling (the lower sub-plot of Figure 2f) displays the maximum difference is about 5%.

The average fraction of laterally and vertically transported non-mare component is 0.07 and 0.03, respectively (Figure 2c and d). The greater average abundance of laterally transported non-mare component indicates the generally higher efficiency of lateral mixing. But it is notable that for a given area of interest, the evaluation of the relative magnitude of the lateral versus vertical mixing needs to take its geologic context into account. For example, if the area is close to the recently-formed impact crater, lateral mixing could become dominant; if the mare material is known to be only thin, the influence of vertical mixing may increase.

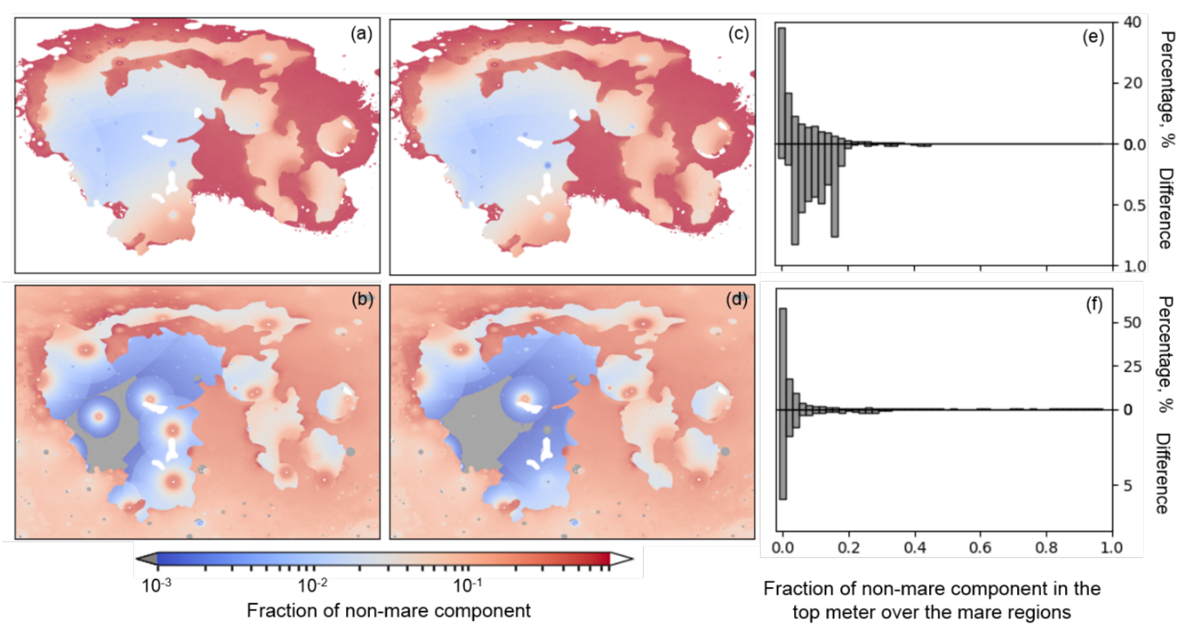

Figure 2 The distribution of non-mare material in the top 5 m. In the first scenario the mare material is emplaced instantaneously (first column, a and b); in the second scenario, it is emplaced by continuous

flooding with time (second column, c and d). (a) and (c) present the abundance of non-mare material that is laterally; (b) and (d) show the abundance of non-mare component that was vertically excavated from the beneath. The upper sub-plots of (e) and (f) present histograms of laterally and vertically transported non-mare abundance of the mare regions when the mare material is emplaced instantaneously, and their lower sub-plot the absolute differences of the percentage caused by the continual filling

4.3. Varying parameters concerning mare filling

Given the uncertainty in the flux of mare filling, simulations with varying setting of mare fillings are run to investigate the major factors affecting the non-mare mixing. The parameters studied include the thickness of mare deposits, the cessation time of the major mare filling and the peak time of eruption. To better compare the results, the sequence of impact craters remains the same. Only the studied parameter is varied, the values of all other parameters are identical to those described in section 2.2 in each simulation. Table 1 summarizes the simulations shown in this section.

Table 1 Simulations with varying parameters concerning mare fillings.

Parameters studied	Mare thickness	Cessation time of the major mare fillings	Peak time of eruption (Ga)
Mare thickness	H_{DeHon} 1/5 H_{DeHon} 1.5 H_{DeHon}	t_{end}	3.8
Cessation time of the major mare fillings	H_{DeHon}	t_{end} t'_{end} t''_{end}	3.8
Peak time of eruption	H_{DeHon}	t_{end}	3.8 3.3

Parameter I: Mare thickness

Estimates of total volume of mare deposit vary significantly. The implicit assumption of the crater-geometry approach that De Hon applied is that all the flooded craters were originally formed on pristine basin floors before any lava had been erupted. The volume estimates are therefore minimum values. Du et al. (2019) found that mare thickness derived from measurements of buried craters were systematically over-estimated because the topographic degradation of the impact craters was not considered. After taking degradation into account, they found that the median thickness was 105 m, which is nearly 5× thinner than H_{DeHon} described in section 2.2 (Figure 1b). In contrast, Gong et al. (2016) used GRAIL gravity data to estimate average mare thickness and found it to be 740 m, which is close to 1.5× thicker than H_{DeHon}.

Both simulations with the thinner (1/5 H_{DeHon}) and thicker (1.5 H_{DeHon}) maria are performed. The statistical non-mare abundance is shown in Figure 3 (the spatial distribution is presented in Figure S4 in the supplementary file). It is seen that the abundance of laterally transported material is not affected by the mare volume, but the vertically transported non-mare component is significantly altered. Since the underlying non-mare component is more easily excavated from the thinner mare deposit, the average abundance of vertically-transported non-mare component on the surface increases by 110%. For the thicker mare infill, the abundance of vertically transported material decreases by 40%.

Parameter II: cessation time of the major mare filling

Given the same total deposit of mare material, as the onset of the mare basalt is taken to be the basin formation age (the upper limit of volcanic eruptions, Ivanov & Melosh 2003), a later cessation time of volcanic eruptions leads to a lower lava eruption flux (i.e., the thinner mare deposit of each mare eruption). To investigate its influence, the simulations with the later cessation time (t'_{end} and t''_{end} in Table 2) are performed. The value of t'_{end} is obtained when the fraction of area of mare deposits younger than a certain age relative to the whole mare region is taken to be 2/3 (rather than ½, t_{end}); The value of t''_{end} is taken from the age of the youngest mare units of each region representing an extreme simulation.

Table 2 The cessation time of the main flooding among different mare regions.

Mare[1]	t_{end}, Ga[2]	t'_{end}, Ga[3]	t''_{end}, Ga[4]
Oceanus Procellarum	3.4	3.0	1.2
Frigoris	3.5	3.5	2.6
Humorum	3.5	3.5	2.9
Nectaris	3.6	3.5	3.4
Fecunditatis	3.6	3.5	3.4
Tranquillitatis	3.6	3.5	3.4
Serenitatis	3.5	3.3	2.4
Crisium	3.3	3.1	2.7
Imbrium	3.3	3.1	2.0

[1] The ages of geologic units of the Mare Crisium, the Mare Nectaris and the Mare Fecunditatis are derived from Hiesinger, van der Bogert, *et al.,* 2011 and Hiesinger *et al.* 2008, and Hiesinger *et al.* 2006, respectively. The others are taken from Hiesinger, Head, *et al.* 2011; [2] More than half of each mare region is covered with volcanic material older than t_{end}; [3] More than two thirds of each mare region is covered with volcanic material older than t'_{end}. [4] t''_{end} is the age of the youngest mare unit of each mare region.

The later cessation time extends the time when laterally transported non-mare material is being buried by the emplaced volcanic material. The volume of laterally-transported non-mare component in the near surface would therefore be less. As seen from Figure 3, in the near surface, when the cessation time of mare flooding is taken to be t'_{end} and t''_{end}, the abundance of the laterally transported non-mare component is 45% and 50% less relative to the estimate shown in Figure 2d, respectively (the spatial distributions are shown in Figure S5).

The later emplacement not only buried the more laterally transported non-mare component, but also the more late-excavated non-mare component caused by the vertical transport. The concentration of vertically transported non-mare component is therefore also less. When the cessation time of mare flooding is taken to be t'_{end} and t''_{end}, its average fraction is decreased by 33% and 40%, respectively (Figure 3 and Figure S6).

Parameter III: peak time of eruption

To investigate the influence from a varying eruption flux, the simulation is performed with a later volcanic eruption peak at 3.3 Ga (instead of 3.8 Ga). Since the abundance of the laterally transported non-mare component depends on the cessation time of the volcanic eruptions, its concentration on the surface is unchanged (Figure 3 and Figure S6).

The younger volcanic peak indicates that the volume (i.e. thickness) of the old volcanic eruption is less. Therefore, in the early period, there would be more vertically transported non-mare being excavated to the near-surface, some of which could be finally delivered to the top surface on present day by the cumulative impact mixing. The simulation results (Figure 3), however, show that the increased amount of the vertically transported non-mare (<1%) is too less to significantly alter the material composition in the top surface.

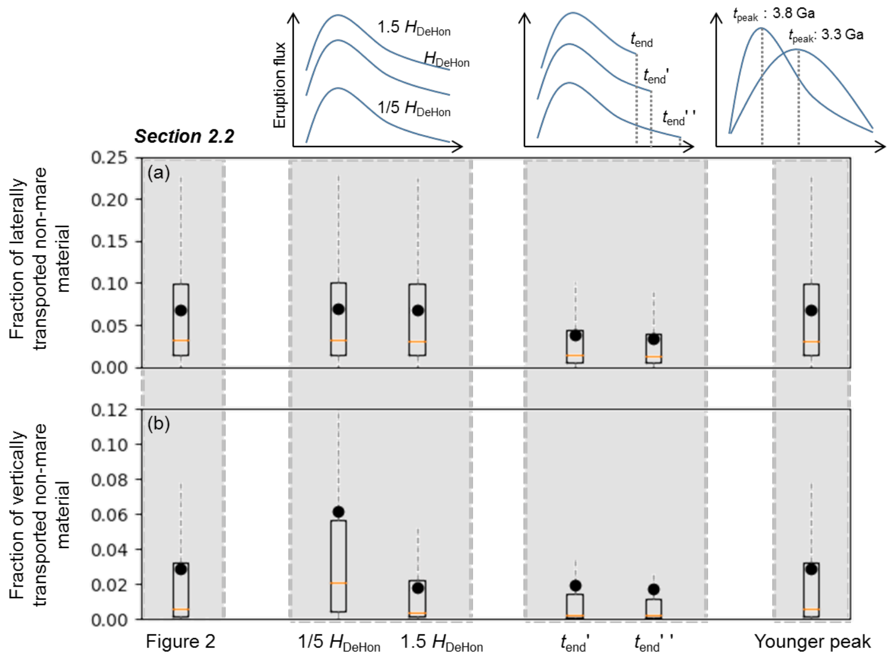

Figure 3 The fraction of laterally (a) and vertically (b) transported non-mare material with varying parameters concerning mare filling in the top 5 m. The results based on the different studied parameters are indicated by four grey zones. For better comparison, the first zone shows the results based on the parameters described in section 2.2 (with mare thickness, H_{DeHon}; cessation time of mare filling, t_{end}; peak time of mare filling, 3.8 Ga). The second, third and fourth zone show the results for other values of mare thickness, cessation and peak time of mare filling, respectively (the parameters are summarized in the Table 1). The schematics above the grey zones illustrate the differences of the studied parameters. The non-mare distribution is shown as box-and-whisker plots. The inside red lines are the median value and the upper and lower boundaries of the boxes are the first and third quantile. The ends of the whiskers represent 99% of data. The black dots represent the mean values.

In summary, on the lateral transport, only the cessation time of the major mare filling has a significant influence. Vertical transport is strongly influenced by both infill thickness variations and the cessation time. The timing of the peak volcanic activity does not exert a significant influence. The non-mare abundance with respective to the simulations of difference parameters is presented in Table S1.

5. Spatial distribution of non-mare component

5.1. Overall features

Because of local impact mixing, the regional distribution of the non-mare component varies with the different random spatial configuration of the generated impact craters in simulations. By taking an average of the results from ten simulations where the spatial configuration of generated craters is different, the regional differences, especially the non-mare enriched zones caused by vertical transport, are averaged out and the general features of non-mare material concentration are obtained (Figure 4).

The spatial distribution of the total non-mare material including both laterally and vertically transported non-mare component in the near surface (the top 5 m) is shown in Figure 4a. Since the regional enrichment in the non-mare component is averaged out, the distribution in each mare region is relatively homogeneous. In addition, it can be seen that throughout the mare regions the non-mare component is present. This is consistent with the results from orbital X-ray instruments, which demonstrated that the admixture of non-mare components is a ubiquitous feature over the entire mare surface (Trombka *et al.*, 1974; Rhodes, 1977; Prettyman *et al.*, 2006).

The older mare surfaces accumulate more non-mare material. The non-mare component over the Mare Tranquillitatis, Fecunditatis, and Nectaris regions showing the more reddish and lighter color is more abundant than that of Oceanus Procellarum and the Mare Serenitatis, Imbrium and Crisium regions. In addition, the boundary of mare and highland regions is generally clear but that of the mare regions where volcanism ceased early is relatively fuzzy, such as Mare Frigoris, Tranquillitatis and Fecunditatis.

The histogram of the non-mare fraction of all the mare regions in the top 5 m (Figure 4b) shows that if most of the mare regions have filled mare material about 500 m in thickness since the formation of basins, the average and median fractions of non-mare component over all the mare regions are both about 0.1. Half of the mare regions possess a non-mare component fraction between 0.05 and 0.15. The mare regions with non-mare fraction smaller than 0.1 are mainly distributed in the Mare Crisium region and the inner parts of Oceanus Procellarum and Mare Imbrium. This results not only from their late volcanic filling, but also from the long distances between the rim and the central regions.

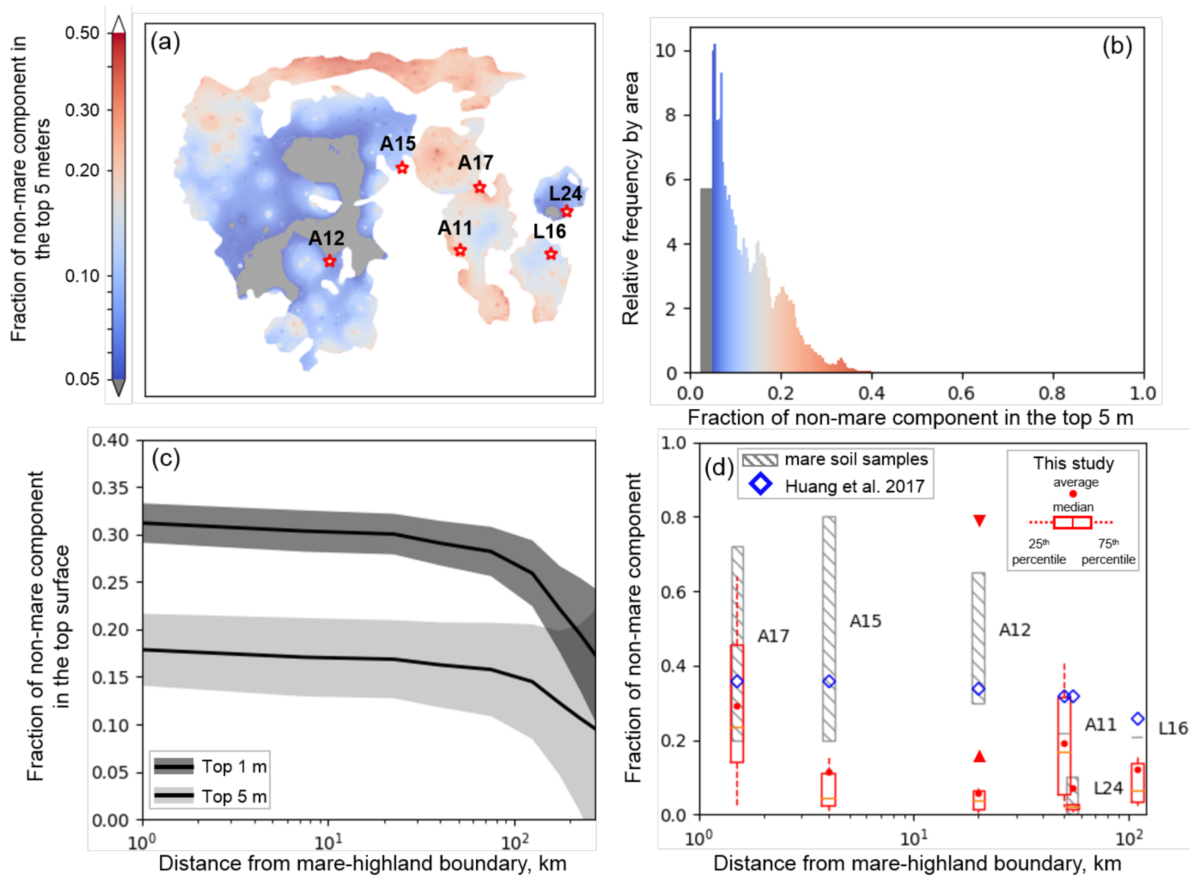

Figure 4 Averaged non-mare material abundance in the top 5 m based on multiple simulations. (a) Spatial distribution of the non-mare component. Red stars indicate the location of Apollo (A) and Luna (L) sampling sites. (b) Histogram of the non-mare component abundance in the top 5m by area over the mare regions. The sum of the bars' value is 100%. (c) Average distribution of non-mare component in the top 1 and 5 m with the distance from mare-highland contact. The black curves indicate the average values and the upper and lower bands of the plots (grey zones) are defined by the 95% confidence intervals from the Monte Carlo simulation results. (d) Non-mare material abundance at the Apollo and Luna sampling sites (Bence & Grove 1978; Rhodes 1977), and its distribution with the distance from the mare-highland boundary. The grey bars with slashes represent the chemical estimate of the lunar soil samples. The blue diamonds are the median abundance from Huang et al. (2017). The red symbols are the results of this study where the points indicate the mean value. The box-and-whisker plots are presented for the better comparison with Huang et al.'s results, where the inside red lines are the median values and the upper and lower boundaries of the boxes are the first and third quantile. The red triangle and the red inverted triangle are the predicted non-mare fraction at A12 when the very early cessation time of mare filling (0.1 Ga after the basin formation) and when the formation of Copernicus Crater (0.8 Ga, 98 km in diameter) is considered, respectively (all the other parameters are the same as those in section 2.2).

5.2. Distribution with the distance from the mare-highland boundary

The fraction of non-mare component at varying distance from mare-highland boundary is calculated by taking the average value of the non-mare fraction of each mare region at the given distance. In the top 5m, the average fraction of the total non-mare material, i.e. including both laterally and vertically transported non-mare material, within 100 km is both about 0.2; between

100 km and 200 km, the non-mare abundance quickly decreases; on the more internal mare regions, the fraction is smaller than 0.1.

The average composition in the top 5 m is regarded to be comparable with that of the lunar surface regolith where the material is homogeneously distributed due to the long-term gardening of small impacts. But for a young surface, such as the youngest geologic unit in Oceanus Procellarum with an age of 1.2 Ga (Hiesinger, Head, *et al.,* 2011), only the very top surface has been well-mixed. The calculated average non-mare abundance in the top meter (Figure 4c) indicates that a fresh surface without intensive mixing could possess higher abundance of non-mare component.

6. Non-mare concentration at sampling sites

This section focuses on the material composition at the sampling sites, to test whether our model is able to reproduce these observations. The results on the basis of multiple simulations weaken the influence of local impact mixing. The calculated average non-mare distribution (Figure 4a) provides expectation values for the spatial composition, although we understand any particular impact configuration will show local differences. Based on the composition of the background surface, the non-mare abundance at the sampling sites is predicted (Table 3).

Figure 4d (red points) shows the expected fraction of the non-mare material of Apollo 11, 12, 15, 17 and Luna 16, 24 sampling sites in the near surface, and in relation to the distance from the mare-highland boundary. All these sampling sites are located near (<~100 km) the mare-highland contact where we expected a weak correlation with the distance. Apollo 11, 17 and Luna 16 are located in Mare Tranquillitatis, at the contact of Mare Tranquillitatis and Serenitatis, and in the Fecunditatis regions, respectively. The volcanic cessation time of these regions was relatively early, resulting in the higher abundance of non-mare component, with a non-mare component fraction of up to ~0.3. The Apollo 15, 12, and Luna 24 sampling sites are located on the Mare Imbrium, Oceanus Procellarum, and the Mare Crisium surfaces, where the volcanic cessation time was later leading to a less non-mare component (~0.1).

The non-mare abundance as a function of distance from the mare-highlands boundary and at the sampling sites were also predicted by Huang et al. (2017). The median values of their results at the sampling site are shown in Figure 4d (blue diamonds). The results of Huang et al. (2017) display no clear relationship between the non-mare abundance and the distance which is consistent with this study, but the non-mare abundance calculated by Huang et al. is generally higher and more comparable with the average composition predicted for the very top surface by our model (Figure 4c). For better comparison, the predicted median values of non-mare abundance of this study are also presented (the red box-and-whisker plot; Table 3). It is seen that both the average and median abundance of non-mare component are smaller than Huang et al's estimate. This can at least in part be explained by the assumptions in the model of Huang et al.: They divided the lunar surface into mare (4 km in thickness) and non-mare zones and took this as the initial status of the model. They did not consider the varying cessation time of mare flooding among the different mare regions and did not involve the continuous mare filling that would bury the early-transported non-mare material, decreasing its abundance. In addition, as indicated in the Figure 4c, the top surface is expected to possess a higher abundance of non-mare material. Huang et al.

calculated the abundance of non-mare material of the very top surface (the uppermost millimeter(s)) which could result in the greater non-mare abundance than this study (the upper meters of the lunar surface material). The process of regolith gardening was contained in Huang et al's model. Such a process would make the material, especially of the top surface (Figure 6 in Huang et al. 2017), homogeneously distributed diluting the non-mare concentration. Even though such a process is not considered in this study, our predicted non-mare abundance is still less than Huang et al's estimate. It may indicate that other factors, such as the sampling depth and the burial by the mare material, have a greater influence on the surface non-mare concentrations. Li and Mustard (2000) also calculated the non-mare abundance through an anomalous diffusion model, but only a narrow zone of the mare/highland boundaries was analyzed. Their results showed that the non-mare fraction quickly decreased from ~0.5 to ~0.2 over 5 km (the mixing-zone). Due to the limit of our model's resolution (5 km), although the drop of the non-mare concentration is not presented in this study (Figure 4), our estimates both in the top one (~0.2) and the top five (~0.3) meters near the mare/highland boundary are consistent with Li and Mustard's results.

Table 3 Non-mare fraction at the sampling sites.

Sampling sites	Chemically estimate[1]	This study[2]		Huang et al. (2017)
		Average	Median[3]	Median
A11	0.2	0.19	$0.17_{0.06}^{0.32}$	0.36
A12	0.3 – 0.7	0.06	$0.04_{0.01}^{0.07}$	0.36
A15	0.2 – 0.8	0.12	$0.04_{0.03}^{0.11}$	0.34
A17	0.1 – 0.7	0.29	$0.24_{0.14}^{0.64}$	0.32
L16	0.2	0.12	$0.07_{0.03}^{0.14}$	0.32
L24	0 – 0.1	0.07	$0.02_{0.01}^{0.02}$	0.26

[1] Rhodes 1977, Bence & Grove 1978; [2] parameters concerning mare flooding are taken to be: mare thickness: H_{DeHon}; the cessation time of the major filling: t_{end}; the peak time of mare eruption: 3.8 Ga;[3] the upper and the lower limit indicate the first and the third quantile.

Grey bars in Figure 4d present the abundance of the non-mare component in the soil samples of Apollo 11, 12, 15, 17 and Luna 16, 24 (Rhodes 1977). The model-predicted non-mare abundance and the measurements of the mare soil samples are then compared:

Apollo 15/17: Both Apollo 15 and 17 samples were collected from multiple stations with the different geologic settings, and thus the non-mare concentrations display widely varying ranges of non-mare concentration. Rhodes *et al.* (1974) classified the Apollo 17 soils samples into three compositional groups. Each one related to a specific geologic setting: valley floor type, south massif type and north massif type. The south massif type soils contain abundant non-mare material with a fraction up to ~0.75 (e.g. Korotev and Kremser 1992), which is much greater than that of the valley floor type soils (~0.2). Similarly to the Apollo 17 soil samples, the Apollo 15 soil samples were found to be dominated by two types (Apennine Front and Apennine base) and the non-mare fraction ranges from about 0.2 to 0.8 (Duncan 1975). As can be seen from Figure 3d, the model-predicted non-mare abundance falls at the lower range of the chemically estimated abundance in the mare soil samples. Given that the sampling site is adjacent to the highland massifs which present the similar chemical composition (KREEPy) with those non-mare samples (Korotev, 1976; Laul *et al.*, 1978), downslope transport by slumping of nearby highlands could be the most plausible process enriching the non-mare abundance of the collected samples.

Apollo 12: The measurements of different Apollo 12 sub-samples also present a wide range of non-mare fraction from 0.3 to 0.7 which is greater than the model-predicted concentration (~0.05). Such a great non-mare abundance (the inverted red triangle in Figure 4d) may be obtained when the very early cessation time of mare-filling is considered in our model (e.g., 0.1 Ga after the basin formation). However, given the KREEP background of the landing site, such an early cessation time of mare-filling is unlikely. The role of other factors is likely more important. The sampling site is close to the late-formed Copernicus crater (390 km north of the site; Wilhelms 1987). According to the orientation of the bright rays of the Copernicus crater, the ejecta material has been believed to be derived from Copernicus crater. The non-mare material entrained in the ejecta of Copernicus could have been spread across the sampling site; in the meanwhile, the high-velocity ejecta could have excavated a certain amount of the underlying non-mare component (Huang et al. 2017; Quaide *et al.*, 1971; Schonfeld and Meyer Charles, 1972). Multiple simulations with the formation of Copernicus crater (800 Ma, 96 km in diameter) are also performed. The results show that if all the other parameters remain the same as those in section 2.2, the non-mare fraction at A12 is increased by a factor of two (the red triangle in Figure 4d). This is still less than both the results of the chemical estimate and Huang et al. A plausible explanation is that the distal ejecta is taken to be continuously distributed so that the spatial geometry of crater rays that were included in Huang et al are not considered. The continuously distributed distal ejecta could be regarded as the consequence of prolonged impact mixing. However, given the young age of Copernicus crater, most of its rays are well-preserved, and thus its influence on the A12 sites could be more significant than we predict.

Apollo 11/Luna 24: The sampling site is far away from the highland-mare boundary and no obvious disturbance of the young ejecta is observed. The model-predicted non-mare fraction of the Apollo 11 and Luna 24 soil samples is ~0.2 and ~0.1, respectively, which falls within the range of the chemical estimates. It indicates that the non-mare component in these soil samples has been mixed with both laterally and vertically transported non-mare material caused by the cumulative impact mixing.

Luna 16: The model-predicted abundance of the non-mare component is less than the chemical estimate of the samples. This may indicate either that the Mare Crisium mare deposit is thinner than 500 m or that the mare surface is older than 3.3 Ga (t_{end} in Table 2).

For the Apollo 11, 15 and Luna 16 samples, rays from Theophilus, Aristarchus or Autolycus, and Langrunus or Tarunius have been proposed as the sources for the highland non-mare components, respectively (Duncan *et al.*, 1975; Schonfeld, 1975). Taking the Apollo 11 sampling site as an example, it is ~380 km (~7.6 radii) away from Theophilus crater (99 km in diameter). The ray length of Theophilus crater can be estimated to be ~950 km (Elliott et al. 2018), so that some of its distal ejecta might have deposited at the Apollo 11 sampling site. If the scaling law of ejecta thickness distribution is extrapolated to this distance, the thickness of Theophilus ejecta at the Apollo 11 sampling is about 1 m. The ratio of the amount of local material to that of ejecta is estimated to be ~3, that is, the fraction of ejecta is about 25%. This is comparable with the chemically estimated value of ~20%. However, the bright ray of Theophilus ejecta has been degraded and is hardly detectable on the present day. It is difficult to determine whether the Apollo 11 sampling site is really located on the ray deposit. If it is, the calculation of the local ejecta thickness indicates that the non-mare component in the samples is mainly derived from Theophilus ejecta. The new look at the Apollo 11 regolith which suggested the more mixing of non-mare component (>20%; Korotev and Gillis, 2001) may further support the deposit of the Theophilus ejecta.

In addition to the impact mixing, some other factors could also affect the non-mare abundance at the sampling sites, such as very young mare lava flows. Due to their small volume, they are typically regionally restricted and can be detected based on spectral data (e.g., the spectral ratios of Clementine imaging data used for the definition of the basaltic units; Hiesinger, Head et al. 2011). In addition, thorough studies of soils samples (e.g., Apollo 17; Rhodes 1974) suggested that the less coherent anorthositic (highland) material was preferentially sampled. Therefore, the sampling strategy could also have led to a bias towards a higher abundance of non-mare material resulting in the difference between the predicted abundance and the chemical estimate of the samples.

It should be mentioned that the abundance of non-mare material is predicted on the basis of the given model parameters including the mare thickness (H_{DeHon}), the cessation (t_{end}) and peak time (3.8 Ga) of mare flooding. Varying these values would change the predicted absolute value of non-mare abundance, but would not significantly change relative abundance among the areas covered with different amount of mare material.

For the Apollo 11 and Luna 24 sampling sites, the consistency between the model-predicted and the chemically estimated non-mare abundance suggests that the mare thickness at both sites is likely to be on the order of 500 m, and that other geologic processes aside from impact mixing did not play a significant role.

7. Conclusions

Lunar mare soil samples from the Apollo and Luna missions contain non-mare component (Rhodes, 1977). To investigate the possible origin and distribution of the contained non-mare component, a numerical model was developed to trace the diffusion of non-mare material, where both the vertical and lateral mixing are recorded to investigate their evolving features. The volcanic flux is the most important parameter, but it is not well constrained (e.g., the total mare volume and the onset and end of eruptions). The abundance of non-mare material is therefore calculated for various possible scenarios.

The laterally and vertically-derived non-mare component display different diffusion features. The distribution of the laterally transported non-mare material is relatively homogeneous and closely related to the distance to the mare-highland boundary. The majority of it is distributed near the mare-highland boundary, while the central mare areas possess a significantly lower abundance of laterally transported non-mare material. In contrast, the vertically-derived non-mare material is patchily distributed. It is closely related to the distribution of large impact events that could excavate a large amount of the underlying non-mare material to the surface, generating non-mare enriched regions. In addition, we find a higher efficiency of lateral transport than that of vertical transport in general. Those diffusion features of both laterally- and vertically-derived non-mare material could be helpful for the choice of future landing sites that aim to collect deep-seated material and for the interpretation of the source of non-mare component in the collected material.

It is found that, across almost the entirety of the mare regions of the Moon, a non-mare component is present. If the mare thickness is on the order of 500 m, the average non-mare fraction over the whole mare regions is about 0.1, and half of the areas possess a fraction ranging from 0.05 to 0.15. The mare surfaces with older volcanic cessation times contain more non-mare material, with an average fraction of ~0.3.

We compared our results with the analysis of the collected soil samples, and discuss the most plausible geologic processes that may have altered the non-mare material abundance at the sampling sites. In the Apollo 15 and 17 samples, the downslope slumping and lateral transport from nearby high relief regions are a likely cause for the larger non-mare component. At the Apollo 12 sampling site, the ejecta of the nearby crater Copernicus, that not only delivered a non-mare component but excavated local material, could increase the regional non-mare concentration. The low amount of non-mare material contained in the Apollo 11, Luna 16 and 24 mare soil samples may result from the gradual accumulation of both the lateral and vertical mixing. In addition, the region where Luna 16 landed may have a very thin mare deposit.

In the future, a model involving topographic relief could be further developed to assess the influence of highland slumping. In addition, with greater understanding of the distribution of distal ejecta, the model could consider some realistic young craters of interest, such as crater Copernicus, and get a more reliable picture of non-mare distribution.

Without a well-constrained estimate of volcanic eruption flux, we performed tentative simulations with the varying mare thickness, the peak time of mare eruption and the cessation time of the major mare filling. It is found that on the surface, the total amount of mare deposit can significantly change the abundance of vertically delivered non-mare, but does not influence the abundance of the laterally transported non-mare material; the peak time of mare eruption could not significantly affect the abundance of both laterally and vertically transported component; the cessation time of the major mare fillings is the major factor altering the abundance of laterally transported non-mare material, and it could also affect the fraction of the buried vertically transported non-mare material that had ever been excavated to the near-surface.

Acknowledgments

We gratefully acknowledge David Minton and Noah Petro for their careful reviews of the manuscript and discussions about cratering processes and formation of impact ejecta with Robert Luther. This work was supported by German Research Foundation (DFG) SFB TRR-707 170-1 TP A4. This is TRR 170 contribution 123.

References

Arvidson, R. *et al.* (1975) ‘Horizontal transport of the regolith, modification of features, and erosion rates on the lunar surface’, *The Moon*, 13(1–3), pp. 67–79. doi: 10.1007/BF00567508.

Bence, A. E. and Grove, T. L. (1978) ‘The Luna 24 highland component’, in Mare Crisium: The view from Luna 24, pp. 429–444.

Budney, C. J. and Lucey, P. G. (1998) ‘Basalt thickness in Mare Humorum: The crater excavation method’, *Journal of Geophysical Research: Planets*, 103(E7), pp. 16855–16870. doi: 10.1029/98JE01602.

Dasch, E. J. *et al.* (1987) ‘Isotopic analysis of basaltic fragments from lunar breccia 14321: Chronology and petrogenesis of pre-Imbrium mare volcanism’, *Geochimica et Cosmochimica Acta*, 51(12), pp. 3241–3254. doi: 10.1016/0016-7037(87)90132-3.

Du, J. *et al.* (2019) ‘Thickness of lunar mare basalts: New results based on modeling the degradation of partially buried craters’, *Journal of Geophysical Research: Planets*, 124, pp. 1–30. doi: 10.1029/2018JE005872.

Duncan, A. R. *et al.* (1975) ‘Interpretation of the compositional variability of Apollo 15 soils.’, *Lunar and Planetary Science Conference Proceedings*, 2, pp. 2309–2320.

Elliott, J. R. *et al.* (2018) ‘The length of lunar crater rays explained using secondary crater scaling’, *Icarus*, 312, pp. 231–246. doi: 10.1016/j.icarus.2018.04.015.

Evans, A. J. *et al.* (2016) ‘Identification of buried lunar impact craters from GRAIL data and implications for the nearside maria’, *Geophysical Research Letters*, 43(6), pp. 2445–2455. doi: 10.1002/2015GL067394.

Fa, W. *et al.* (2014) ‘Regolith thickness over Sinus Iridum: Results from morphology and size-frequency distribution of small impact craters’, *Journal of Geophysical Research E: Planets*. doi: 10.1002/2013JE004604.

Fa, W. and Jin, Y. Q. (2010) ‘A primary analysis of microwave brightness temperature of lunar surface from Chang-E 1 multi-channel radiometer observation and inversion of regolith layer thickness’, *Icarus*, 207(2), pp. 605–615. doi: 10.1016/j.icarus.2009.11.034.

Farrand, W. H. (1988) ‘Highland contamination and minimum basalt thickness in northern Mare Fecunditatis’, in *Lunar and Planetary Science Conference Proceedings*, pp. 319–329.

Fischer, E. M. and Pieters, C. M. (1995) ‘Lunar surface aluminum and iron concentration from Galileo solid state imaging data, and the mixing of mare and highland materials’, *Journal of Geophysical Research*, 100(E11), p. 23279. doi: 10.1029/95JE02359.

Gong, S. *et al.* (2016) ‘Thicknesses of mare basalts on the Moon from gravity and topography’, *Journal of Geophysical Research: Planets*, 121(5), pp. 854–870. doi: 10.1002/2016JE005008.

Hawke, B. R. and Bell, J. F. (1982) ‘Remote sensing studies of lunar dark-halo impact craters: preliminary results and implications for early volcanism.’, *Lunar and Planetary Science Conference Proceedings*, 12, pp. 665–678.

Head, J. W. (1976) ‘Lunar volcanism in space and time’, *Reviews of Geophysics*, 14(2), pp. 265–300. doi: 10.1029/RG014i002p00265.

Head, J. W. (1977) ‘Origin of outer rings in lunar multi-ringed basins: evidence from morphology and ring spacing.’, in Roddy, D. ~J., Pepin, R. ~O., and Merrill, R. ~B. (eds) *Impact and Explosion Cratering: Planetary and Terrestrial Implications*, pp. 563–573.

Head, J. W. (1982) ‘Lava flooding of ancient planetary crusts: Geometry, thickness, and volumes of flooded lunar impact basins’, *The Moon and the Planets*, 26(1), pp. 61–88. doi: 10.1007/BF00941369.

Head, J. W. and Wilson, L. (1992) ‘Lunar mare volcanism: Stratigraphy, eruption conditions, and the evolution of secondary crusts’, *Geochimica et Cosmochimica Acta*, 56(6), pp. 2155–2175. doi: 10.1016/0016-7037(92)90183-J.

Head, J. W. and Wilson, L. (2017) ‘Generation, ascent and eruption of magma on the Moon: New insights into source depths, magma supply, intrusions and effusive/explosive eruptions (Part 2: Predicted emplacement processes and observations)’, *Icarus*, 283, pp. 176–223. doi: 10.1016/j.icarus.2016.05.031.

Hiesinger, H. *et al.* (2006) ‘New ages for basalts in Mare Fecunditatis based on crater size-frequency measurements’, *Lunar Planet. Sci. XXXVII*.

Hiesinger, H. *et al.* (2008) ‘Ages of Mare Basalts on the Lunar Nearside: A Synthesis’, in *Lunar and Planetary Science Conference*. (Lunar and Planetary Science Conference), p. 1269.

Hiesinger, H., Head, J. W., *et al.* (2011) ‘Ages and stratigraphy of lunar mare basalts: A synthesis’, *Recent Advances and Current Research Issues in Lunar Stratigraphy*. Geological Society of America Special Paper 477, 477, pp. 1–51.

Hiesinger, H., van der Bogert, C. H., *et al.* (2011) ‘Crater Size-Frequency Distribution Measurements of Mare Crisium’, in *Lunar and Planetary Science Conference*. (Lunar and Planetary Science Conference), p. 2179.

De Hon, R. A. (1974) ‘Thickness of mare material in the Tranquillitatis and Nectaris basins’, in *Lunar and Planetary Science Conference Proceedings*, pp. 53–59.

De Hon, R. A. (1979) ‘Thickness of western mare basalts’, in *Proceedings of the 10th Lunar and Planetary Science Conference*. New York, pp. 2935–2955.

De Hon, R. A. and Waskom, J. D. (1976) ‘Geologic structure of the eastern mare basins.’, *Lunar and Planetary Science Conference Proceedings*, 3, pp. 2729–2746.

Hörz, F. (1978) ‘How thick are lunar mare basalts’, in *Lunar and Planetary Science Conference Proceedings*, pp. 3311–3331.

Hörz, F. *et al.* (1991) ‘Lunar surface processes’, *Lunar sourcebook*. Cambridge Univ. Press Cambridge, pp. 61–120.

Hörz, F., Ostertag, R. and Rainey, D. A. (1983) ‘Bunte Breccia of the Ries: Continuous deposits of large impact craters’, *Reviews of Geophysics*, pp. 1667–1725. doi: 10.1029/RG021i008p01667.

Huang, Y. *et al.* (2017) ‘Heterogeneous impact transport on the Moon’, *Journal of Geophysical Research: Planets*, (122), pp. 1–23. doi: 10.1002/2016JE005160.

Korotev, R. L. (1976) ‘Geochemistry of grain-size fractions of soils from the Taurus-Littrow valley floor’, in *Lunar and Planetary Science Conference Proceedings*, pp. 695–726.

Korotev, R. L. and Gillis, J. J. (2001) ‘A new look at the Apollo 11 regolith and KREEP’, *Journal of Geophysical Research: Planets*, 106(E6), pp. 12339–12353. doi: 10.1029/2000JE001336.

Korotev, R. L. and Kremser, D. T. (1992) ‘Compositional variations in Apollo 17 soils and their relationship to the geology of the Taurus-Littrow site.’, *Lunar and Planetary Science Conference Proceedings*, 22, pp. 275–301.

Laul, J. C. *et al.* (1978) ‘Chemistry and petrology of size fractions of Apollo 17 deep drill core 70009-70006’, in *Lunar and Planetary Science Conference Proceedings*, pp. 2065–2097.

Laul, J. C. and Papike, J. J. (1980) ‘The lunar regolith-comparative chemistry of the Apollo sites’, in *Lunar and Planetary Science Conference Proceedings*, pp. 1307–1340.

Li, L. and Mustard, J. F. (2000) ‘Compositional gradients across mare-highland contacts: Importance and geological implication of lateral transport’, *Journal of Geophysical Research: Planets*, 105(E8), pp. 20431–20450. doi: 10.1029/1999JE001168.

Liu, T. *et al.* (2019) ‘Regolith mixing by impacts : Lateral diffusion of basin melt’, *Icarus*. Elsevier, 321(0019–1035), pp. 691–704. doi: 10.1016/j.icarus.2018.12.026.

Liu, T. *et al.* (2020) ‘Lunar megaregolith mixing by impacts: Spatial diffusion of basin melt and its implications for sample interpretation’, *Icarus*, 339. doi: 10.1016/j.icarus.2019.113609.

Lucey, P. *et al.* (2006) ‘Understanding the Lunar Surface and Space-Moon Interactions’, *Reviews in Mineralogy and Geochemistry*, 60(1), pp. 83–219. doi: 10.2138/rmg.2006.60.2.

McKay, D. *et al.* (1991) ‘The lunar regolith’, in Heiken, G. H., Vaniman, D. T., and French, B. M. (eds) *Lunar Source-Book: A user’s guide to the Moon*. New York: Cambridge University Press, pp. 285–356. doi: 10.1006/icar.1999.6165.

Needham, D. H. and Kring, D. A. (2017) ‘Lunar volcanism produced a transient atmosphere around the ancient Moon’, *Earth and Planetary Science Letters*, 478, pp. 175–178. doi: 10.1016/j.epsl.2017.09.002.

Neukum, G. (1983) ‘Meteoritenbombardement und Datierung Planetarer Oberflaechen’, *Habilitation Dissertation for Faculty Membership, Univ. of Munich*, pp. 1–186.

Nyquist, L. E., Bogard, D. D. and Chi-Yu, S. (2001) ‘Radiometric chronology of the Moon and Mars’, in *The century of space science*. Springer, pp. 1325–1376.

Nyquist, L. E. and Shih, C.-Y. (1992) ‘The isotopic record of lunar volcanism’, *Geochimica et Cosmochimica Acta*, 56(6), pp. 2213–2234. doi: 10.1016/0016-7037(92)90185-L.

Oberbeck, V. R. (1971) ‘A mechanism for the production of lunar crater rays’, *The Moon*, 2(3), pp. 263–278. doi: 10.1007/BF00561880.

Oberbeck, V. R. *et al.* (1975) ‘On the origin of the lunar smooth plains’, *The Moon*, 12(1), pp. 19–54.

Phillips, R. J. *et al.* (1972) ‘Mascons: Progress toward a unique solution for mass distribution’, *Journal of Geophysical Research (1896-1977)*, 77(35), pp. 7106–7114. doi: 10.1029/JB077i035p07106.

Phillips, R. J. and Lambeck, K. (1980) ‘Gravity fields of the terrestrial planets: Long-wavelength anomalies and tectonics’, *Reviews of Geophysics*, 18(1), pp. 27–76. doi: 10.1029/RG018i001p00027.

Prettyman, T. H. *et al.* (2006) ‘Elemental composition of the lunar surface: Analysis of gamma ray spectroscopy data from Lunar Prospector’, *Journal of Geophysical Research: Planets*, 111(E12). doi: 10.1029/2005JE002656.

Quaide, W. *et al.* (1971) ‘Investigations of the natural history of the regolith at the Apollo 12 site’, *Lunar and Planetary Science Conference Proceedings*, 2, p. 701.

Rhodes, J. M. (1977) ‘Some Compositional Aspects of Lunar Regolith Evolution’, *Philosophical Transactions of the Royal Society A: Mathematical, Physical and Engineering Sciences*, 285(1327), pp. 293–301. doi: 10.1098/rsta.1977.0068.

Rhodes, J. M. *et al.* (1974) ‘The relationships between geology and soil chemistry at the Apollo 17 landing site.’, *Lunar and Planetary Science Conference Proceedings*, 2, pp. 1097–1117.

Ryder, G. and Spudis, P. (1980) ‘Volcanic rocks in the lunar highlands.’, in Merrill, R. ~B. and Papike, J. ~J. (eds) *Lunar Highlands Crust*, pp. 353–375.

Schonfeld, E. (1975) ‘Component Abundances in Apollo 15 Soils and Breccias by the Mixing Model Technique’, in *Lunar and Planetary Science Conference*, p. 712.

Schonfeld, E. and Meyer, Jr. (1972) 'The abundances of components of the lunar soils by a least-squares mixing model and the formation age of KREEP', *Lunar and Planetary Science Conference Proceedings*, 3, p. 1397.

Schultz, P. H. and Spudis, P. D. (1979) ‘Evidence for ancient mare volcanism.’, *Lunar and Planetary Science Conference Proceedings*, 3, pp. 2899–2918.

Simon, S. B., Papike, J. J. and Laul, J. C. (1982) ‘The lunar regolith-Comparative studies of the Apollo and Luna sites. Petrology of soils from Apollo 17, Luna 16, 20, and 24’, in *Lunar and Planetary Science Conference Proceedings*, pp. 371–388.

Solomon, S. C. and Head, J. W. (1980) 'Lunar Mascon Basins: Lava filling, tectonics, and evolution of the lithosphere', *Reviews of Geophysics*, 18(1), pp. 107–141. doi: 10.1029/RG018i001p00107.

Stöffler, D. (2006) 'Cratering history and lunar chronology', *Reviews in Mineralogy and Geochemistry*, 60(1), pp. 519–596. doi: 10.2138/rmg.2006.60.05.

Taylor, L. A. *et al.* (1983) 'Pre-4.2 AE mare-basalt volcanism in the lunar highlands', *Earth and Planetary Science Letters*, 66, pp. 33–47. doi: 10.1016/0012-821X(83)90124-3.

Thomson, B. J. *et al.* (2009) 'A new technique for estimating the thickness of mare basalts in Imbrium Basin', *Geophysical Research Letters*, 36(12). doi: 10.1029/2009GL037600.

Trombka, J. I. *et al.* (1974) 'Lunar elemental analysis obtained from the Apollo gamma-ray and X-ray remote sensing experiment'.

Warren, P. H. and Wasson, J. T. (1977) 'Pristine nonmare rocks and the nature of the lunar crust.', *Lunar and Planetary Science Conference Proceedings*, 2, pp. 2215–2235.

Whitten, J. L. and Head, J. W. (2015a) 'Lunar cryptomaria: Mineralogy and composition of ancient volcanic deposits', *Planetary and Space Science*, 106, pp. 67–81. doi: https://doi.org/10.1016/j.pss.2014.11.027.

Whitten, J. L. and Head, J. W. (2015b) 'Lunar cryptomaria: Physical characteristics, distribution, and implications for ancient volcanism', *Icarus*, 247, pp. 150–171. doi: https://doi.org/10.1016/j.icarus.2014.09.031.

Wilhelms, D. E. (1987) *The geologic history of the Moon*, *U.S. Geological Survey Professional Paper*. doi: 10.1007/s13398-014-0173-7.2.

Williams, K. K. and Zuber, M. T. (1998) 'Measurement and Analysis of Lunar Basin Depths from Clementine Altimetry', *Icarus*, 131(1), pp. 107–122. doi: 10.1006/icar.1997.5856.

Wilson, L. and Head, J. W. (2017) 'Generation, ascent and eruption of magma on the Moon: New insights into source depths, magma supply, intrusions and effusive/explosive eruptions (Part 1: Theory)', *Icarus*, 283, pp. 146–175. doi: 10.1016/j.icarus.2015.12.039.

Wood, J. A. (1970) 'Petrology of the lunar soil and geophysical implications', *Journal of Geophysical Research*, 75(32), pp. 6497–6513. doi: 10.1029/JB075i032p06497.